




# Combining Multifrequency Magnetic Resonance Elastography With Automatic Segmentation to Assess Renal Function in Patients With Chronic Kidney Disease

Qiumei Liang, MS,<sup>1,2</sup> Haiwei Lin, MS,<sup>3</sup> Junfeng Li, MS,<sup>1</sup>  Peiyin Luo, MS,<sup>1</sup> Ruirui Qi, MS,<sup>1</sup> Qiuyi Chen, MS,<sup>1</sup>  Fanqi Meng, BS,<sup>1</sup> Haodong Qin, MS,<sup>4</sup> Feifei Qu, PhD,<sup>4</sup> Youjia Zeng, MD,<sup>5</sup> Wenjing Wang, MD,<sup>5</sup> Jiandong Lu, MD,<sup>5</sup> Bingsheng Huang, PhD,<sup>3\*</sup> and Yueyao Chen, MD<sup>1\*</sup> 

**Background:** Multifrequency MR elastography (mMRE) enables noninvasive quantification of renal stiffness in patients with chronic kidney disease (CKD). Manual segmentation of the kidneys on mMRE is time-consuming and prone to increased interobserver variability.

**Purpose:** To evaluate the performance of mMRE combined with automatic segmentation in assessing CKD severity.

**Study Type:** Prospective.

**Participants:** A total of 179 participants consisting of 95 healthy volunteers and 84 participants with CKD.

**Field Strength/Sequence:** 3 T, single shot spin echo planar imaging sequence.

**Assessment:** Participants were randomly assigned into training ( $n = 58$ ), validation ( $n = 15$ ), and test ( $n = 106$ ) sets. Test set included 47 healthy volunteers and 58 CKD participants with different stages (21 stage 1–2, 22 stage 3, and 16 stage 4–5) based on estimated glomerular filtration rate (eGFR). Shear wave speed (SWS) values from mMRE was measured using automatic segmentation constructed through the nnU-Net deep-learning network. Standard manual segmentation was created by a radiologist. In the test set, the automatically segmented renal SWS were compared between healthy volunteers and CKD subgroups, with age as a covariate. The association between SWS and eGFR was investigated in participants with CKD.

**Statistical Tests:** Dice similarity coefficient (DSC), analysis of covariance, Pearson and Spearman correlation analyses.  $P < 0.05$  was considered statistically significant.

**Results:** Mean DSCs between standard manual and automatic segmentation were 0.943, 0.901, and 0.970 for the renal cortex, medulla, and parenchyma, respectively. The automatically quantified cortical, medullary, and parenchymal SWS were significantly correlated with eGFR ( $r = 0.620$ ,  $0.605$ , and  $0.640$ , respectively). Participants with CKD stage 1–2 exhibited significantly lower cortical SWS values compared to healthy volunteers ( $2.44 \pm 0.16$  m/second vs.  $2.56 \pm 0.17$  m/second), after adjusting age.

View this article online at [wileyonlinelibrary.com](https://onlinelibrary.wiley.com/doi/10.1002/jmri.29719). DOI: 10.1002/jmri.29719

Received Sep 28, 2024, Accepted for publication Jan 10, 2025.

\*Address reprint requests to: Y.C., Department of Radiology, The Fourth Clinical Medical College of Guangzhou University of Chinese Medicine (Shenzhen Traditional Chinese Medicine Hospital), No. 1, Fuhua Road, Shenzhen 518033, Guangdong, China. E-mail: [drchenyueyao@163.com](mailto:drchenyueyao@163.com), or B.H., Medical AI Lab, School of Biomedical Engineering, Medical School, Shenzhen University, No. 1066, Xueyuan Avenue, Nanshan District, Shenzhen 518055, Guangdong, China. E-mail: [huangbs@gmail.com](mailto:huangbs@gmail.com)

Q.L. and H.L. contributed equally as the first authors.

From the <sup>1</sup>Department of Radiology, The Fourth Clinical Medical College of Guangzhou University of Chinese Medicine (Shenzhen Traditional Chinese Medicine Hospital), Shenzhen, China; <sup>2</sup>Department of Radiology, The Sixth School of Clinical Medicine, the Affiliated Qingyuan Hospital (Qingyuan People's Hospital), Guangzhou Medical University, Qingyuan, China; <sup>3</sup>Medical AI Lab, School of Biomedical Engineering, Medical School, Shenzhen University, Shenzhen, China; <sup>4</sup>MR Research Collaboration, Siemens Healthineers, Shanghai, China; and <sup>5</sup>Department of Nephrology, The Fourth Clinical Medical College of Guangzhou University of Chinese Medicine (Shenzhen Traditional Chinese Medicine Hospital), Shenzhen, China

Additional supporting information may be found in the online version of this article

This is an open access article under the terms of the [Creative Commons Attribution-NonCommercial-NoDerivs](https://creativecommons.org/licenses/by-nc-nd/4.0/) License, which permits use and distribution in any medium, provided the original work is properly cited, the use is non-commercial and no modifications or adaptations are made.

**Conclusion:** mMRE combined with automatic segmentation revealed abnormal renal stiffness in patients with CKD, even with mild renal impairment.

### Plain Language Summary

The renal stiffness of patients with chronic kidney disease varies according to the function and structure of the kidney. This study integrates multifrequency magnetic resonance elastography with automated segmentation technique to assess renal stiffness in patients with chronic kidney disease. The findings indicate that this method is capable of distinguishing between patients with chronic kidney disease, including those with mild renal impairment, while simultaneously reducing the subjectivity and time required for radiologists to analyze images. This research enhances the efficiency of image processing for radiologists and assists nephrologists in detecting early-stage damage in patients with chronic kidney disease.

**Level of Evidence:** 2

**Technical Efficacy:** Stage 2

J. MAGN. RESON. IMAGING 2025;61:2543–2555.

Chronic kidney disease (CKD) is a global public health problem.<sup>1</sup> A recent cross-sectional survey showed that the prevalence of CKD in China is 8.7%, affecting approximately 82 million people.<sup>2</sup> CKD is characterized by a progressive loss of kidney function, which can eventually lead to end-stage kidney disease, requiring kidney transplantation and hemodialysis to sustain life. For patients with CKD, early diagnosis of renal impairment and accurate assessment of disease severity are important in order for clinicians to tailor more effective treatment strategies to slow the disease process.<sup>3,4</sup>

The estimated glomerular filtration rate (eGFR) calculated from serum creatinine (Scr) is the most commonly used clinical indicator for evaluating kidney function and serves as the standard for clinical staging.<sup>5</sup> However, many factors such as body muscle mass and protein intake influence the eGFR,<sup>6,7</sup> resulting in low sensitivity and specificity. Also, the eGFR does not allow assessment of the function of a single kidney. Therefore, a method that can provide an early, accurate, and noninvasive evaluation of changes in kidney function as well as detailed anatomical information is needed.

Pathological changes that occur during a decline in renal function, such as interstitial fibrosis and glomerulosclerosis,<sup>8</sup> can alter renal stiffness; therefore, stiffness may be used as an imaging biomarker to assess renal function. MR elastography (MRE) is a technique that enables assessment of tissue stiffness by measuring the velocity of shear waves passing through the tissue and is well-established for assessing liver fibrosis.<sup>9,10</sup> Several studies have reported the feasibility of MRE for diagnosing CKD<sup>11–16</sup>; however, the results are inconsistent. Multifrequency MRE (mMRE) provides complementary information to the composite elastogram by acquiring wavefields at multiple frequencies compared with those of conventional single-frequency MRE, yielding images with higher spatial resolution and signal-to-noise ratio in a faster time.<sup>17–19</sup> Thus, mMRE may be more suitable for investigating small and heterogeneous organs such as the kidneys.

Conventional image analysis methods require manually outlining regions of interest (ROIs), which is time-consuming and subjective. Some studies have developed algorithms to automatically segment the liver based on MRE images and

to quantify the elasticity values.<sup>20,21</sup> Therefore, the aim of this study was to evaluate the performance of mMRE combined with automatic segmentation in assessing CKD severity.

## Materials and Methods

### Study Population

From March 2023 to February 2024, 95 healthy volunteers and 84 participants with CKD were consecutively recruited at Shenzhen Traditional Chinese Medicine Hospital. This prospective study adhered to the Declaration of Helsinki and was approved by the Ethics Committee of Shenzhen Traditional Chinese Medicine Hospital (K2023-047-02). Each participant signed written informed consent (Fig. 1).

The inclusion criteria for healthy volunteers were (1) had undergone regular physical examinations showing no previous history of renal diseases, diabetes, hypertension, or vascular diseases; and (2) no history of taking nephrotoxic drugs in the past 3 months. Participants with CKD must have met the “Kidney Disease: Improving Global Outcomes” (KDIGO) definition of CKD,<sup>5</sup> which is renal structural or functional impairment for  $\geq 3$  months. The exclusion criteria were (1) transplanted kidneys; (2) renal malignancy; (3) large ( $>2$  cm) or multiple benign occupying lesions of the kidneys (eg, angiomyolipoma, polycystic kidneys); (4) renal stones with hydronephrosis; and (5) poor quality of renal mMRE images.

### Clinical Parameters

Scr, uric acid (UA), urea, total protein-to-creatinine ratio (TPCR), and urinary albumin-to-creatinine ratio (UACR) were recorded for participants with CKD. The eGFR of participants with CKD was calculated using the CKD Epidemiology Collaboration equation based on Scr.<sup>22</sup> Participants with CKD were classified into three subgroups based on CKD stage<sup>5</sup>: CKD stage 1–2 (mild renal impairment,  $\text{eGFR} \geq 60 \text{ mL/min/1.73 m}^2$ ); CKD stage 3 (moderate renal impairment,  $30 \text{ mL/min/1.73 m}^2 \leq \text{eGFR} < 60 \text{ mL/min/1.73 m}^2$ ); and CKD stage 4–5 (severe renal impairment,  $\text{eGFR} < 30 \text{ mL/min/1.73 m}^2$ ).

### mMRE Acquisition

All participants underwent mMRE after 4 hours without drinking or eating. The mMRE examination was performed on a 3 T MRI scanner (MAGNETOM Prisma, Siemens Healthineers, Erlangen, Germany) using an 18-channel body phased-array coil. mMRE was

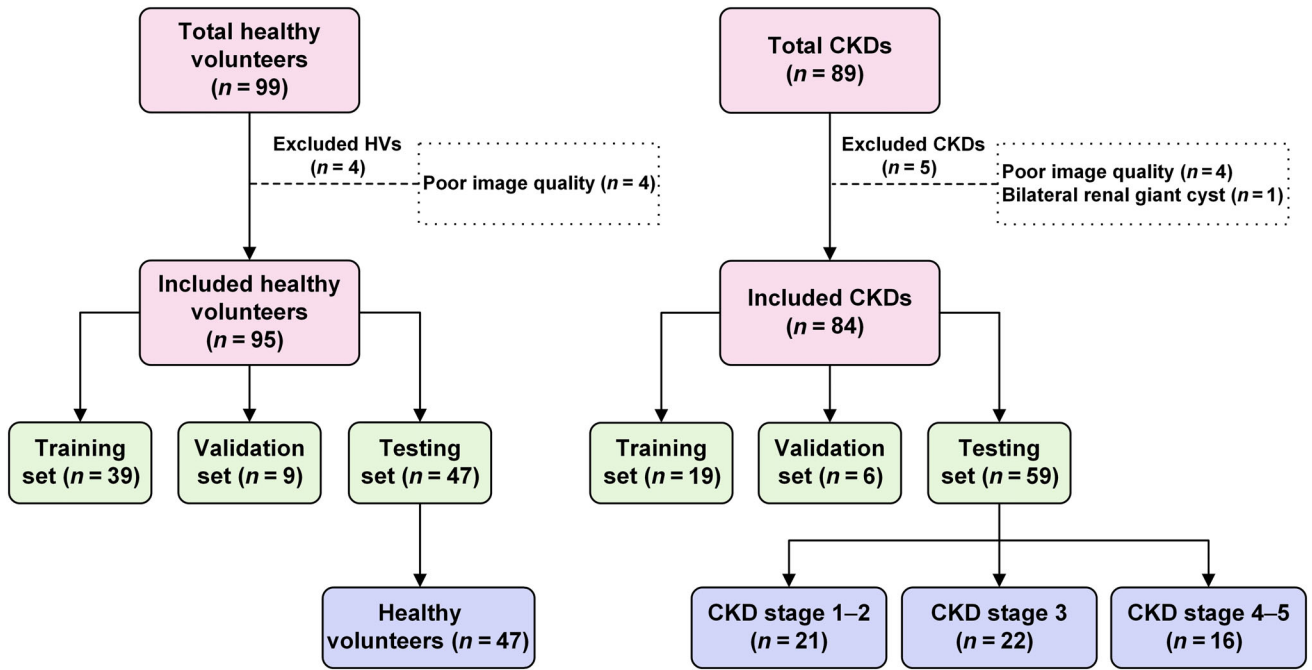


FIGURE 1: Study flowchart. CKD = chronic kidney disease.

performed using single shot spin echo planar imaging sequence. The mMRE images were acquired by positioning one passive actuator beneath each kidney. The actuators driven by compressed air, generated vibrations at four frequencies ranging from 40 to 70 Hz, with increments of 10 Hz and an air pressure of 0.5–0.7 bar. Twenty-five coronal slices with resolution of  $2.5 \times 2.5 \times 2.5 \text{ mm}^3$  were acquired in 5 minutes during free breathing. Further imaging parameters were: repetition time (TR) = 2450 msec; echo time (TE) = 56 msec; field of view (FOV) of  $250 \times 250 \text{ mm}^2$  (matrix size:  $104 \times 104$ ) parallel imaging with a GRAPPA factor of 2; MEG amplitude = 45 mT/m. MEG frequency = 48.36 Hz for vibration frequencies of 40, 50, and 60 Hz; MEG frequency = 52.41 Hz for vibration frequencies of 70 Hz.

### mMRE Data Processing

mMRE data were postprocessed using the wave number-based multifrequency dual elasto-visco (k-MDEV) reconstruction algorithm to produce magnitude images (Fig. 2i–l) and shear wave speed (SWS) maps (Fig. 2m–p) as in the studies of Dittmann et al and Marticorena Garcia et al.<sup>23–25</sup> SWS maps can be used to measure the SWS value (in m/second), also known as the elasticity value, which reflects the tissue stiffness, and will henceforth be referred to as “elastograms.” Larger SWS values, indicate harder tissue. Magnitude images are T2-weighted magnitude images that show the anatomy of the kidneys. The reconstruction algorithm for mMRE images utilized in this study can be available at [www.bioqic-apps.charite](http://www.bioqic-apps.charite).

### Construction of Automatic Segmentation Model of the Renal Cortex, Medulla, and Parenchyma Based on mMRE Images

**DATA PREPARATION.** Participants were randomly divided into training ( $n = 58$ ), validation ( $n = 15$ ), and test ( $n = 106$ ) sets,

representing approximately 30%, 10%, and 60% of the data, respectively. The training set was used to train the deep-learning model for image segmentation; the validation set was used to determine the optimal model for segmenting the cortex, medulla, and parenchyma. In the test set, the optimal model was applied for image segmentation followed by SWS values quantification.

**STANDARD MANUAL SEGMENTATION CREATION.** The standard manual segmentation involved delineating the cortex, medulla, and parenchyma (including both cortex and medulla) on the coronal magnitude images datasets of all 179 participants. It was exclusively employed to establish the automatic segmentation model, not for the quantification of renal SWS values. The radiologist (Q.L., with 8 years of MRI experience) using the ITK-SNAP medical image annotation tool (version 3.8.0; [www.itksnap.org](http://www.itksnap.org)) performed the standard manual segmentation. To measure the inter- and intra-observer variability of the standard manual segmentation, 30 cases randomly selected from the test set were re-delineated by Q.L. and J.L. (a radiologist with 2 years of MRI experience).

**NETWORK TRAINING.** The nnU-Net structure was used which automatically configures the preprocessing, network architecture, and training procedures on the original training dataset without manual parameter tuning, making it adaptable to various medical imaging datasets.<sup>26</sup> For data preprocessing, the training data were cropped to retain only nonzero regions to reduce computational costs. All images were resampled to a median voxel spacing of  $2.5 \times 2.5 \times 2.5 \text{ mm}^3$  to learn spatial semantics, then the z-scores were normalized for each participant to standardize the input scale for the model.

During training, the batch size was set to 2, and the patch size was  $28 \times 104 \times 104$ . Consequently, the size of the input four-dimensional image block was  $2 \times 28 \times 104 \times 104$ . The model

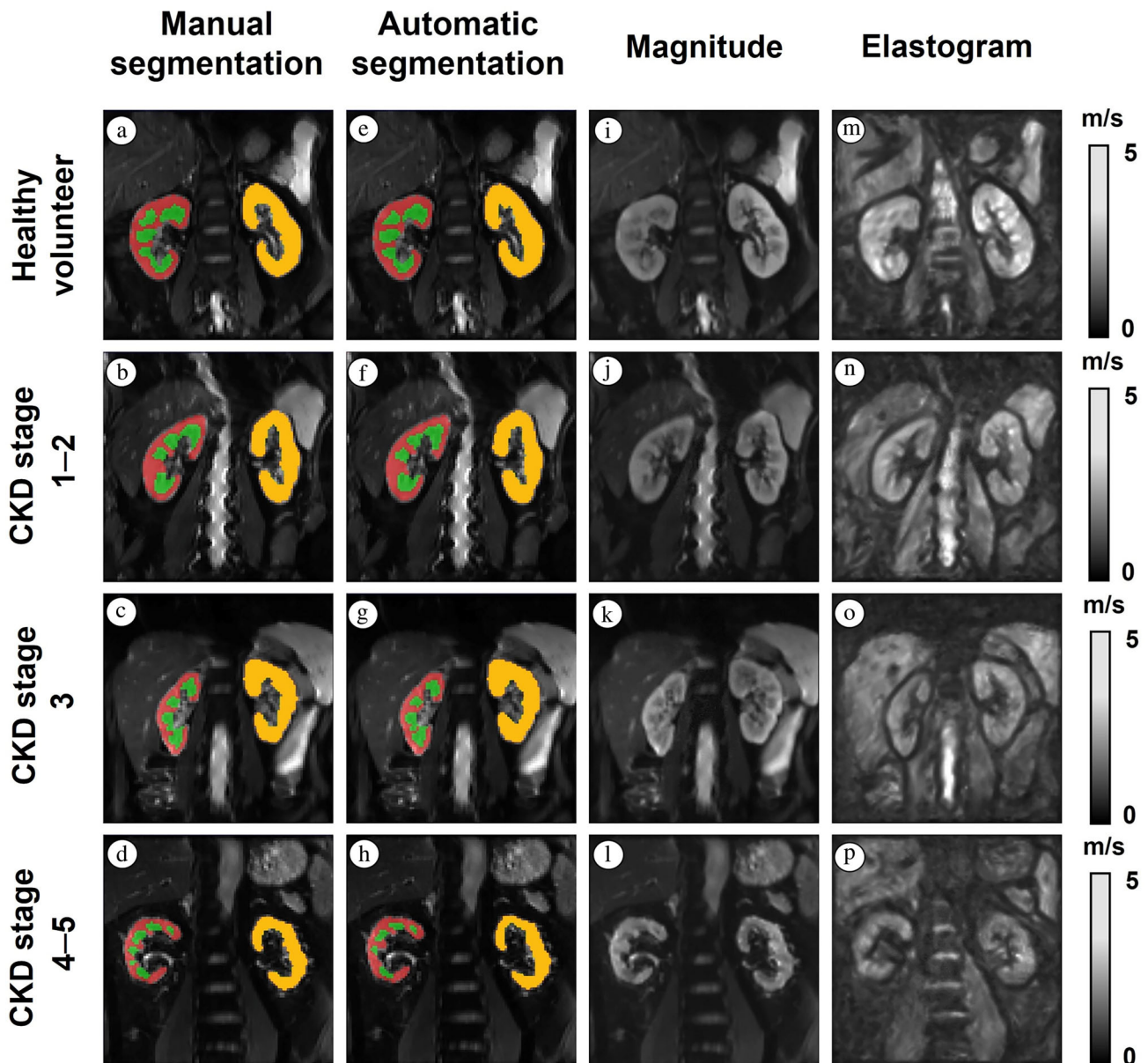


**FIGURE 2:** Magnitude images and elastograms from renal mMRE and the corresponding standard manual and automatic segmentations. Using standard manual segmentation (a–d) as the reference, the automatic segmentation accurately identified the renal cortex, medulla, and parenchyma in the healthy volunteers (e; DSC: 0.971, 0.950, 0.984), CKD stage 1–2 (f; DSC: 0.969, 0.941, 0.984) and CKD stage 3 (g; DSC: 0.922, 0.906, 0.955) groups, but some medulla could not be identified in the CKD stage 4–5 (h; DSC: 0.900, 0.836, 0.954) group. The magnitude images showed that the boundary between the cortex and medulla of the kidneys remained clear in the healthy volunteers, CKD stage 1–2, and CKD stage 3 groups, while it was relatively blurred in the CKD stage 4–5 group (i–l). The elastograms showed a gradual trend in decreasing signal intensity in the kidneys as the disease severity increased (m–p). Red: cortex; green: medulla; yellow: parenchyma. mMRE = multifrequency magnetic resonance elastography; CKD = chronic kidney disease.

training was conducted in three-dimensional (3D) full-resolution mode for 1000 epochs, with 250 iterations per epoch.

Data augmentation techniques, including rotation, scaling, Gaussian noise, Gaussian blur, brightness, contrast, low-resolution simulation, gamma correction, and mirroring, were applied in real-time during training to enhance the model's generalization and robustness. The network weights were updated by minimizing the sum of the cross-entropy loss and Dice similarity coefficient (DSC) loss. The segmentation model was trained on an Ubuntu 16.04.5

operating system equipped with 2 GeForce GTX 1080 Ti and 20 Intel(R) Xeon(R) CPU E5-2650 v3 @ 2.30GHz.

**PERFORMANCE EVALUATION.** The DSC is widely used to measure the similarity between the prediction and reference values. The 95% Hausdorff distance (95HD) was used to measure the segmentation performance of boundaries and eliminates the impact of a very small subset of the outliers.<sup>27</sup>



### Quantification of Renal SWS Values Based on mMRE

To automatically quantify the test set, the automatic segmentation results (Fig. 3a) were matched to the corresponding elastograms (Fig. 3b) to obtain the renal SWS values (cortical, medullary, and parenchymal). Notably, images at the marginal level of the kidney were susceptible to spinal and intestinal gases, leading to potential deformation. Therefore, we referred to relevant literature and selected three consecutive sections in the center of the kidney to quantify the SWS values.<sup>28</sup>

In order to compare the automatic quantification developed in this study with the conventional manual quantification, two radiologists (Q.L. and J.L., with 8 and 2 years of MRI experience, respectively) manually quantify renal SWS values by referring to the delineation method of Marticorena Garcia et al.<sup>24</sup> They selected three consecutive slices in the center of the kidney from the magnitude images without knowledge of the participants' clinical data, and manually delineated the ROIs of the renal cortex, medulla, and parenchyma (Fig. 3c) using ImageJ (Java 1.8.0.322 [64-bit]).<sup>29</sup> Note that conventional manual quantification (Fig. 3c) of the renal cortex excluded renal columns, while automatic quantification included them (Fig. 3a). The ROIs in each slice included as much of the target tissue as possible while avoiding the renal edges and renal sinus blood vessels. In addition, due to the subjectivity of manual selection, the slices may differ from those chosen by the automatic segmentation model. These ROIs were matched to the corresponding elastograms (Fig. 3b) to obtain the renal SWS values (cortical, medullary, and parenchymal), and recorded as radiologist 1 and radiologist 2. One of the radiologists (Q.L.) repeated this process after a 1-week interval and was recorded as radiologist 1–2.

Finally, the cortical, medullary, and parenchymal SWS values of the left and right kidneys were averaged. In addition, to assess the effectiveness of automatic quantification in increasing efficiency, we measured the total processing time required to obtain one participant's renal SWS values using automatic quantification and one radiologist (Q.L.) using conventional manual quantification separately. This included the time needed to delineate the ROIs of renal cortex, medulla, and parenchyma on the magnitude image and the ROIs were matched to the elastogram to obtain the SWS values.

### Statistical Analysis

Measurement data were tested for normality. Normally distributed data are expressed as means  $\pm$  standard deviation; non-normally distributed data are expressed as medians (interquartile range). Categorical data are expressed as frequencies (percentages). Statistical analysis was performed using IBM SPSS statistics version 22.0, MedCalc version 20.022, and GraphPad Prism version 9.0.0.  $P < 0.05$  was considered statistically significant. All statistical analyses in this study were performed in the test set.

Intraclass correlation coefficient (ICC) was used to evaluate the consistency of the renal SWS values. The ICC criteria were as follows: ICC  $< 0.5$  indicated poor consistency;  $0.5 \leq \text{ICC} < 0.75$  indicated moderate consistency;  $0.75 \leq \text{ICC} < 0.9$  indicated good consistency; ICC  $> 0.9$  indicated excellent consistency.<sup>30</sup> Independent-sample  $t$  tests were used to compare the automatically quantified cortical and medullary SWS values. Paired-sample  $t$  tests were used to compare renal SWS values from bilateral kidneys. Analysis of covariance (ANCOVA) with age as a covariate was used to compare the automatically quantified renal SWS values of healthy volunteers and participants with CKD. ANCOVA with age as a covariate was used to compare renal SWS values among groups in

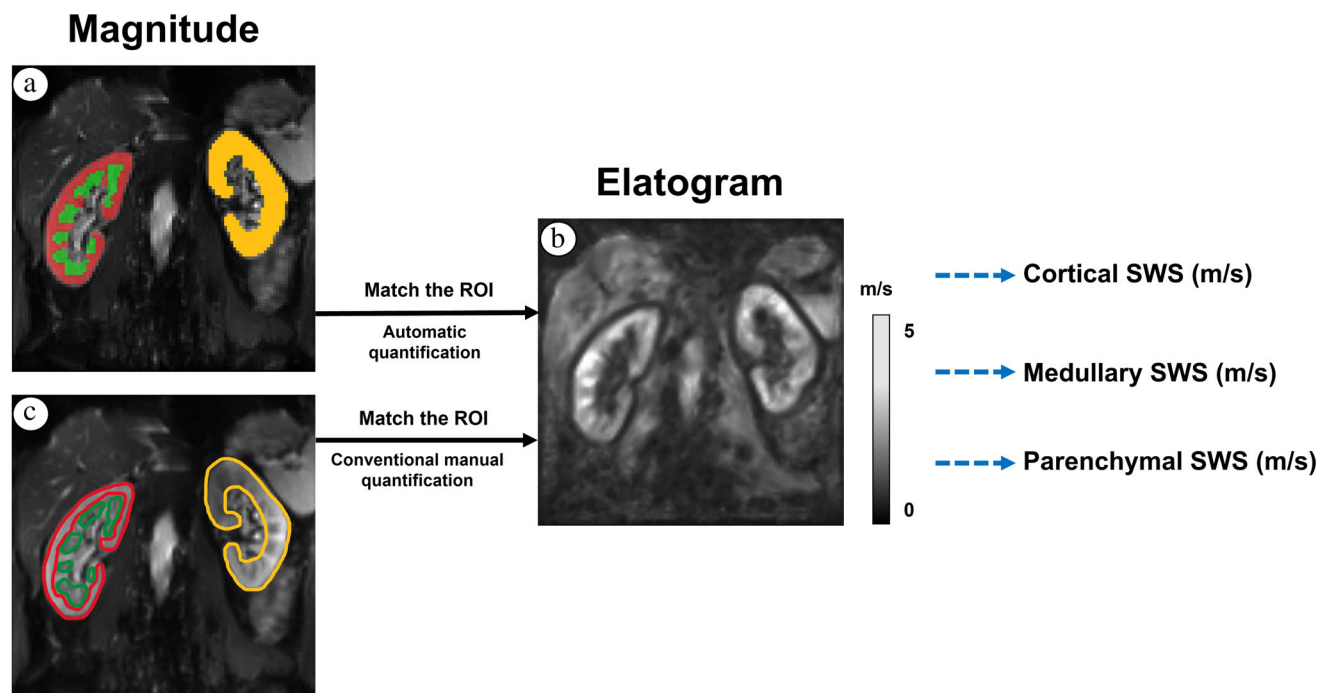


FIGURE 3: Schematic diagram of the automatic quantification and conventional manual quantification. Red: cortex; green: medulla; yellow: parenchyma. mMRE = multifrequency MR elastography; ROI = region of interest; SWS = shear wave speed.

the test set (healthy volunteers vs. CKD stage 1–2 vs. CKD stage 3 vs. CKD stage 4–5), and post hoc Bonferroni correction was applied for pairwise comparisons. Pearson correlation analysis was used to assess the association between eGFR, UA, and renal SWS values. Spearman correlation analysis was used to assess the correlations between Scr, urea, TPCR, UACR, and renal SWS values. Receiver operating characteristic (ROC) curve analysis was used to evaluate the diagnostic performance of the renal SWS values obtained by automatic quantification and by two radiologists using conventional manual quantification for identifying participants with CKD. The area under the curve (AUC) was calculated with the 95% confidence interval (95% CI), cutoffs, sensitivities, and specificities. DeLong's test was used to determine the significance of AUC differences.

## Results

### Study Population

Between March 2023 and February 2024, 188 participants were enrolled (99 healthy volunteers and 89 participants with CKD). Among them, four healthy volunteers and four participants with CKD were excluded due to poor mMRE image quality and one participant with CKD was excluded due to bilateral large renal cysts (Fig. 1). Finally, 179 participants (95 healthy volunteers and 84 participants with CKD) were included in analysis. Among them, 59 participants with CKD (mean age:  $45.47 \pm 12.47$  years; 40 men) and 47 healthy volunteers (mean age:  $35.28 \pm 12.40$  years; 17 men) were included in the test set. The 59 participants with CKD were classified into CKD stage 1–2 ( $n = 21$ ), CKD stage 3 ( $n = 22$ ), and CKD stage 4–5 ( $n = 16$ ) groups (Fig. 1). Table 1 lists the detailed characteristics of the participants in the test set. Table S1 in the Supplemental Material displays the attributes of the participants in training, validation, and test sets.

### Consistency of the Renal SWS Values

The total processing time for automatic quantification was greatly shorter than conventional manual quantification ( $5.15 \pm 0.04$  seconds vs.  $25.87 \pm 2.23$  minutes).

The ICCs for conventional manual quantification of the cortical, medullary, and parenchymal SWS values by the two radiologists at the same time were 0.697 (95% CI: 0.585–0.783), 0.608 (95% CI: 0.473–0.715), and 0.668 (95% CI: 0.547–0.761), respectively. The ICCs for conventional manual quantification of the cortical, medullary, and parenchymal SWS values by the radiologist (Q.L.) 1 week later were 0.810 (95% CI: 0.731–0.867), 0.780 (95% CI: 0.690–0.846), and 0.750 (95% CI: 0.648–0.825), respectively.

The ICCs between automatic and conventional manual quantification of renal SWS values were less than 0.5, as detailed in Table S2 in the Supplemental Material.

### Performance of the Automatic Segmentation Model

Table 2 shows that the automatic segmentation results for the cortex, medulla, and parenchyma were good in the healthy volunteers, CKD stage 1–2 and CKD stage 3 groups (DSC: 0.912–0.978; 95HD: 2.126–2.547) and relatively poor in the CKD stage 4–5 group (DSC: 0.798–0.940; 95HD: 2.629–3.120).

The inter- and intra-observer variability of the standard manual segmentation for 30 randomly chosen examples is displayed in Table S3 in the Supplemental Material. The results show low variability.

### Anatomical Regional Variations in Renal SWS Values

There was no significant difference between the left and right kidneys in the automatically quantified cortical, medullary, and parenchymal SWS values (healthy volunteers:  $P = 0.480$ ,  $P = 0.290$ , and  $P = 0.458$ , respectively; CKD:  $P = 0.190$ ,  $P = 0.283$ , and  $P = 0.205$ , respectively). Cortical SWS values were significantly greater than those of the medulla in the healthy volunteers ( $2.56 \pm 0.17$  m/second vs.  $2.36 \pm 0.17$  m/second). SWS values did not significantly differ between the cortex and medulla in the participants with CKD ( $2.30 \pm 0.23$  m/second vs.  $2.22 \pm 0.25$  m/second; mean difference, 0.08 [95% CI:  $-0.01$  to  $0.17$ ];  $P = 0.062$ ).

### Correlation between Renal SWS Values and Renal Function Indices

In participants with CKD, the automatically quantified cortical, medullary, and parenchymal SWS values were significantly correlated with eGFR ( $r = 0.620$ ,  $r = 0.605$ , and  $r = 0.640$ , respectively). However, the correlations between TPCR, UACR, UA, and renal SWS values showed no statistically significant differences (TPCR:  $P = 0.353$ ,  $P = 0.748$ , and  $P = 0.680$ , respectively; UACR:  $P = 0.473$ ,  $P = 0.650$ , and  $P = 0.821$ , respectively; UA:  $P = 0.098$ ,  $P = 0.522$ , and  $P = 0.174$ , respectively). Table 3 displays the correlation results in detail.

### Renal SWS Values Between Healthy Volunteers and CKD Participants With Different Stages

Even after adjusting for age as a covariate, significant differences in renal SWS values were still observed between healthy volunteers and participants with CKD, and among healthy volunteers and all subgroup of CKD. In addition, cortical SWS values are lower in participants with CKD stage 1–2 than in healthy volunteers, while medullary and parenchymal SWS values do not differ statistically significantly from those of healthy volunteers, as shown in Fig. 4. Table 4 shows the detailed automatically quantified cortical, medullary, and parenchymal SWS values for each group of the test

TABLE 1. Characteristics of the Study Population in the Test Set

Characteristics	Healthy Volunteers	CKD	Subgroups of CKD			$P^a$	$P^b$
			CKD Stage 1–2	CKD Stage 3	CKD Stage 4–5		
Number ( <i>n</i> )	47	59	21	22	16	NA	NA
Age (year)	35.28 ± 12.40	45.47 ± 12.47	38.57 ± 8.06	46.91 ± 12.87	52.56 ± 12.64	<0.001	0.002
Male (%)	17 (36%)	40 (68%)	14 (67%)	16 (73%)	10 (63%)	0.012 <sup>c</sup>	0.793 <sup>c</sup>
BMI (kg/m <sup>2</sup> )	22.83 ± 2.88	23.77 ± 3.74	24.21 ± 4.73	23.68 ± 3.57	23.32 ± 2.43	0.458	0.775
HR (bpm)	NA	83.83 ± 11.36	85.38 ± 11.44	82.86 ± 11.10	83.13 ± 12.11	NA	0.743
Systolic blood pressure (mmHg)	NA	128.82 ± 19.27	124.43 ± 17.49	125.59 ± 15.71	139.38 ± 22.82	NA	0.036
Diastolic blood pressure (mmHg)	NA	84.53 ± 10.97	84.81 ± 9.85	82.64 ± 10.79	86.75 ± 12.76	NA	0.524
TPCR (mg/g)	NA	500 (1660)	295 (530)	435 (1030)	2019 ± 1334	NA	0.002 <sup>d</sup>
UACR (mg/g)	NA	321 (1398)	242 (489)	278 (883)	1646 ± 1166	NA	0.005 <sup>d</sup>
UA (μmol/L)	NA	411.78 ± 95.26	427.38 ± 96.63	398.41 ± 94.41	409.69 ± 97.74	NA	0.613
Urea (mmol/L)	NA	7.72 (5.90)	6.51 ± 3.52	8.19 ± 2.63	15.84 ± 7.17	NA	<0.001
Scr (μmol/L)	NA	138.00 (100.00)	93.52 ± 25.70	146.50 ± 28.14	309.75 ± 87.60	NA	<0.001
eGFR (mL/min/1.73 m <sup>2</sup> )	NA	52.73 ± 30.057	84.86 ± 21.63	46.82 ± 8.98	18.69 ± 4.94	NA	<0.001

BMI = body mass index; HR = heart rate; TPCR = total protein-to-creatinine ratio; UACR = urinary albumin-to-creatinine ratio; UA = uric acid; Scr = serum creatinine; eGFR = estimate glomerular filtration rate; CKD = chronic kidney disease; NA = not applicable.

<sup>a</sup> $P$ -values indicated comparisons of the difference among healthy volunteers, CKD stage 1–2, CKD stage 3, and CKD stage 4–5 groups.

<sup>b</sup> $P$ -values indicated comparisons of the overall difference among CKD stage 1–2, CKD stage 3, and CKD stage 4–5 groups.

<sup>c</sup>Differences among groups were tested using the chi-square test.

<sup>d</sup>Differences among groups were tested using the Kruskal–Wallis test.

**TABLE 2. Performance of the Automatic Segmentation Model in the Test Set**

	Healthy Volunteers ( <i>n</i> = 47)	CKD Stage 1–2 ( <i>n</i> = 21)	CKD Stage 3 ( <i>n</i> = 22)	CKD Stage 4–5 ( <i>n</i> = 16)	Total ( <i>n</i> = 106)
Cortical DSC	0.952 ± 0.030	0.957 ± 0.016	0.949 ± 0.024	0.888 ± 0.095	0.943 ± 0.049
Medullary DSC	0.920 ± 0.044	0.924 ± 0.033	0.912 ± 0.051	0.798 ± 0.202	0.900 ± 0.096
Parenchymal DSC	0.975 ± 0.015	0.978 ± 0.008	0.973 ± 0.013	0.940 ± 0.053	0.970 ± 0.026
Cortical 95HD	2.126 ± 0.927	2.381 ± 0.546	2.159 ± 0.878	2.694 ± 0.417	2.269 ± 0.809
Medullary 95HD	2.500 ± 0.000	2.500 ± 0.000	2.547 ± 0.221	3.120 ± 1.133	2.603 ± 0.491
Parenchymal 95HD	2.486 ± 0.457	2.500 ± 0.000	2.500 ± 0.000	2.629 ± 0.354	2.513 ± 0.334

DSC = Dice similarity coefficient; 95HD = 95% Hausdorff distance; CKD = chronic kidney disease.

set. Figure 2i–p shows magnitude images and elastograms of a healthy kidney and renal softening in the CKD subgroups.

### Diagnostic Performance of mMRE

In differentiating between participants with CKD and healthy volunteers, automatically quantified cortical SWS values showed greater diagnostic performance (AUC: 0.827 [95% CI: 0.741–0.893]) than medullary and parenchymal SWS values (AUCs: 0.680 [95% CI: 0.582–0.767] and 0.780 [95% CI: 0.689–0.855], respectively; Fig. 5a). Radiologist 1 (Q.L.) and radiologist 2 (J.L.) also obtained similar conclusion using conventional manual quantification (Fig. 5c,e).

Only the cortical SWS values demonstrated diagnostic power when automatically quantified renal SWS values were used to identify participants with CKD stage 1–2 and healthy volunteers (AUC, 0.721 [95% CI: 0.599–0.823]), as seen in Fig. 5b,d,f. This performance was poorer than that of radiologist 1 (AUC, 0.747 [95% CI: 0.632–0.862]) but better than that of radiologist 2 (AUC, 0.629 [95% CI: 0.489–0.770]).

Table 5 displays the detailed AUCs, cutoff values, sensitivities, and specificities.

### Discussion

Accurate classification of disease severity in patients with CKD is important in clinical practice.<sup>5</sup> In this study, a well-performing segmentation model of the renal cortex, medulla, and parenchyma was established which yielded renal SWS values that enabled assessment of renal function changes in patients with CKD and identification of early renal function damage.

The segmentation model of the renal cortex, medulla, and parenchyma constructed using 3D nnU-Net based on mMRE images had excellent segmentation performance in healthy volunteers and CKD stage 1–2 and CKD

stage 3 groups, but less good in the CKD stage 4–5 group. The inferior segmentation performance in the CKD stage 4–5 group may be attributed to significantly impaired renal function, resulting in atrophic kidneys and a poorly defined corticomedullary border. Additionally, a previous automatic segmentation study of the renal cortex in healthy volunteers using arterial spin labeling (ASL) images yielded a DSC of 0.78.<sup>31</sup> In contrast, our study achieved a DSC of 0.888 in the more challenging CKD stage 4–5 group, outperforming the prior study. Moreover, the differences in cortical, medullary, and parenchymal SWS values between CKD stage 4–5 and other groups were statistically significant. Consequently, the segmentation performance of the CKD stage 4–5 group remained satisfactory. The low inter- and intra-observer variability of the standard manual segmentation indicates its reliability, which further supports the reliability of the automatic segmentation model.

Most studies on measuring renal elasticity values have used manual measurements and lacked a standard manual outlining technique, resulting in time-consuming and subjective variability throughout the measurement process and a lack of comparability between studies. Our results demonstrate that automatic quantification is much more efficient than conventional manual quantification. The renal SWS values measured by the radiologists showed moderate inter-observer and good intra-observer agreement, but not excellent. Conversely, the automatic quantification was deterministic in all processing steps and provided a 100% reproducible ROI, thus reducing variability in assessing renal SWS values due to subjective differences.

The automatically quantified renal SWS values gradually decreased as the eGFR decreased in patients with CKD, suggesting that the kidneys of patients with CKD soften with the progression of the disease. This finding was similar to the



**TABLE 3. Correlations Between Renal Function Indices and Automatically Quantified Renal SWS Values (n = 59)**

Correlation Group	Pearson <i>r</i> / Spearman $\rho$	<i>P</i>
Cortical SWS and		
eGFR	0.620	<0.001
Scr	−0.675 <sup>a</sup>	<0.001
Urea	−0.338 <sup>a</sup>	0.009
TPCR	−0.124 <sup>a</sup>	0.353
UACR	−0.096 <sup>a</sup>	0.473
UA	0.217	0.098
Medullary SWS and		
eGFR	0.605	<0.001
Scr	−0.572 <sup>a</sup>	<0.001
Urea	−0.169 <sup>a</sup>	0.225
TPCR	0.043 <sup>a</sup>	0.748
UACR	0.061 <sup>a</sup>	0.650
UA	0.085	0.522
Parenchymal SWS and		
eGFR	0.640	<0.001
Scr	−0.654 <sup>a</sup>	<0.001
Urea	−0.258 <sup>a</sup>	0.048
TPCR	−0.055 <sup>a</sup>	0.680
UACR	−0.030 <sup>a</sup>	0.821
UA	0.180	0.174

SWS = shear wave speed; eGFR = glomerular filtration rate; Scr = serum creatinine; TPCR = total protein-to-creatinine ratio; UACR = urinary albumin-to-creatinine ratio; UA = uric acid.

<sup>a</sup>Because Scr, urea, TPCR, and UACR were non-normally distributed, Spearman's test was applied.

results of some recent studies that were also based on mMRE images but used manual measurements to obtain renal SWS values.<sup>11,13,15,16</sup> For example, studies in lupus nephritis and IgA patients have shown a positive correlation between eGFR and mMRE-derived elasticity values.<sup>15,16</sup> Furthermore, several researchers have shown a negative correlation between the pathological parameters of renal fibrosis and the elasticity values.<sup>11,13</sup> However, it was previously thought that tissue and organ stiffness increase with accumulation of the

extracellular matrix.<sup>32</sup> It has been found that a gradual increase in MRE-derived liver elasticity values as the degree of liver fibrosis increases,<sup>33,34</sup> and transplanted kidneys with fibrosis are stiffer than those with stable disease.<sup>35,36</sup> The possible reason for this is that native kidneys have higher blood flow than the liver and transplanted kidneys, and the high blood perfusion may produce a compression force on the surrounding renal tissues.<sup>37</sup> When pathological changes such as interstitial fibrosis and glomerulosclerosis occur in native kidneys, renal blood perfusion gradually decreases, thus reducing the compression on the kidneys to soften them.<sup>38</sup> Although interstitial fibrosis hardens the kidneys, the reduction in renal blood perfusion has a greater effect on renal softening, resulting in a decreased overall kidney stiffness.<sup>15</sup> This hypothesis was verified in a study that combined ASL and MRE to assess fibrosis in patients with diabetic nephropathy, revealing a decline in both renal perfusion and stiffness corresponding to the progression of CKD.<sup>14</sup> In addition, an animal investigation found that the MRE-derived elasticity values of isolated normal porcine kidneys gradually decreased as the perfusion decreased, suggesting that decreasing perfusion could soften the kidneys.<sup>39</sup>

The automatically quantified cortical, medullary, and parenchymal SWS values were lower in patients with CKD than in healthy volunteers. Additionally, the cortical SWS values of patients with CKD stage 1–2 were lower than those of healthy volunteers. Although there were significant age differences between the groups, the differences in SWS values remained statistically significant after adjusting for age as a covariate in ANCOVA. However, in some studies, there were no abnormalities in renal elasticity values in patients with CKD who had mild renal impairment.<sup>12,16</sup> In our study, the significant differences in cortical elasticity values for patients with early stage CKD may be attributed to the higher spatial resolution of mMRE compared with single frequency MRE, which allows accurate anatomical differentiation between the cortex and medulla,<sup>17</sup> along with the objectivity provided by high-performance automatic segmentation, and a larger sample size.

In the application of automatically quantified renal SWS values to identify patients with early renal impairment, only the cortical SWS values showed significant results which were better than that of radiologist 2 and slightly inferior to that of radiologist 1. The difference in diagnostic efficacy may stem from the insufficient intergroup consistency of renal SWS values derived from automatic versus conventional manual quantification. The following reasons may explain the insufficient consistency. First, the segmentation methods of automatic and conventional manual quantification are different. Conventional manual quantification of the renal cortex excludes renal columns. Second, the size and shape of renal

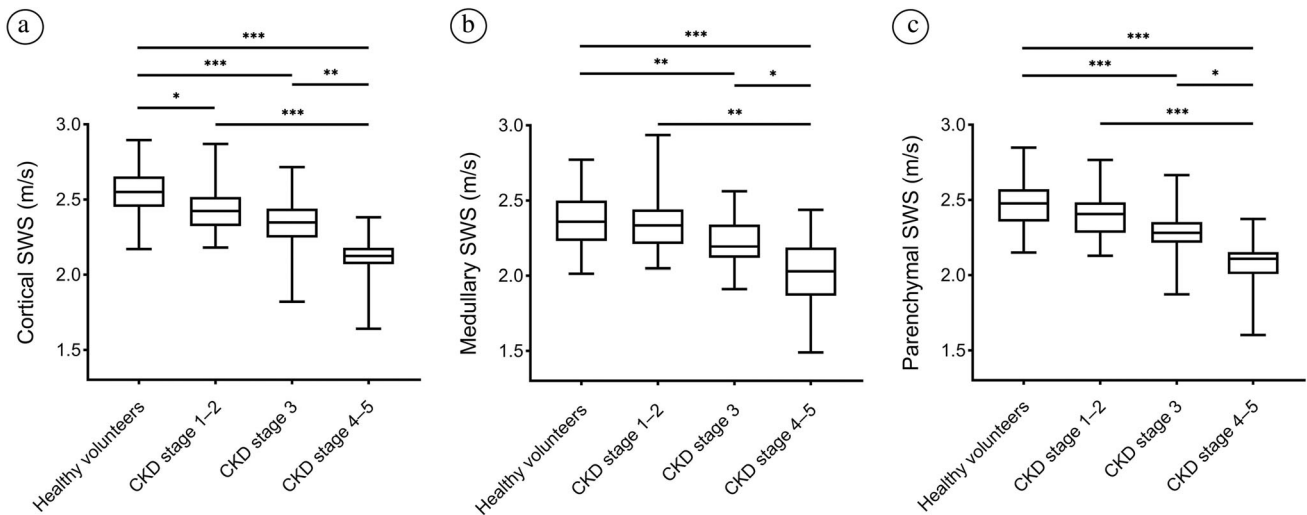


**FIGURE 4:** Comparison of automatically quantified cortical (a), medullary (b), and parenchymal (c) SWS values in healthy volunteers and subgroups of participants with CKD. Only cortical SWS values differed significantly between healthy volunteers and patients with CKD stage 1–2. SWS = shear wave speed; CKD = chronic kidney disease; \* $P < 0.05$ ; \*\* $P < 0.01$ ; \*\*\* $P < 0.001$ .

TABLE 4. Comparison of Automatically Quantified Renal SWS Values in Healthy Volunteers and Participants With CKD							
	Healthy Volunteers ( <i>n</i> = 47)	CKD ( <i>n</i> = 59)	Subgroups of CKD			<i>P</i> <sup>a</sup>	<i>P</i> <sup>b</sup>
			CKD Stage 1–2 ( <i>n</i> = 21)	CKD Stage 3 ( <i>n</i> = 22)	CKD Stage 4–5 ( <i>n</i> = 16)		
Cortical SWS (m/second)	2.56 ± 0.17	2.30 ± 0.23 <sup>c</sup>	2.43 ± 0.16 <sup>c</sup>	2.33 ± 0.20 <sup>c</sup>	2.09 ± 0.18 <sup>c-c</sup>	<0.001	<0.001
Medullary SWS (m/second)	2.36 ± 0.17	2.22 ± 0.25 <sup>c</sup>	2.37 ± 0.21	2.22 ± 0.18 <sup>c</sup>	2.03 ± 0.24 <sup>c-c</sup>	0.006	<0.001
Parenchymal SWS (m/second)	2.48 ± 0.16	2.27 ± 0.22 <sup>c</sup>	2.41 ± 0.16	2.29 ± 0.18 <sup>c</sup>	2.07 ± 0.19 <sup>c-c</sup>	<0.001	<0.001

SWS = shear wave speed; CKD = chronic kidney disease.  
<sup>a</sup>*P*-values indicated comparisons of the difference between healthy volunteers and CKD groups with age as a covariate.  
<sup>b</sup>*P*-values indicated the overall difference among healthy volunteers, CKD stage 1–2, CKD stage 3, and CKD stage 4–5 groups with age as a covariate.  
<sup>c</sup>Versus healthy volunteers,  $P < 0.05$ .  
<sup>d</sup>Versus CKD stage 1–2,  $P < 0.05$ .  
<sup>e</sup>Versus CKD stage 3,  $P < 0.05$ .

ROIs can vary based on the subjective judgment of radiologists. Third, the selected slices vary. The three consecutive slices in the center of the kidney for automatic quantification are established according to algorithmic criteria, while those for conventional manual quantification are selected by radiologists based on their professional expertise. In addition, the cortical SWS values may be sensitive indicators for detecting early renal impairment in patients with CKD, enabling early detection before obvious changes in renal function. Two

reasons may explain why the cortical SWS values were more sensitive than were the medullary SWS values. Firstly, there are differences in the blood supply. The cortex has significantly higher blood perfusion than the medulla, accounting for approximately 90% of the renal blood flow.<sup>37</sup> Renal blood perfusion decreases as CKD progresses, and the cortex is more susceptible; thus, reduced renal blood perfusion may affect cortical stiffness earlier. Secondly, the cortex is responsible for most of the glomerular filtration and excretory

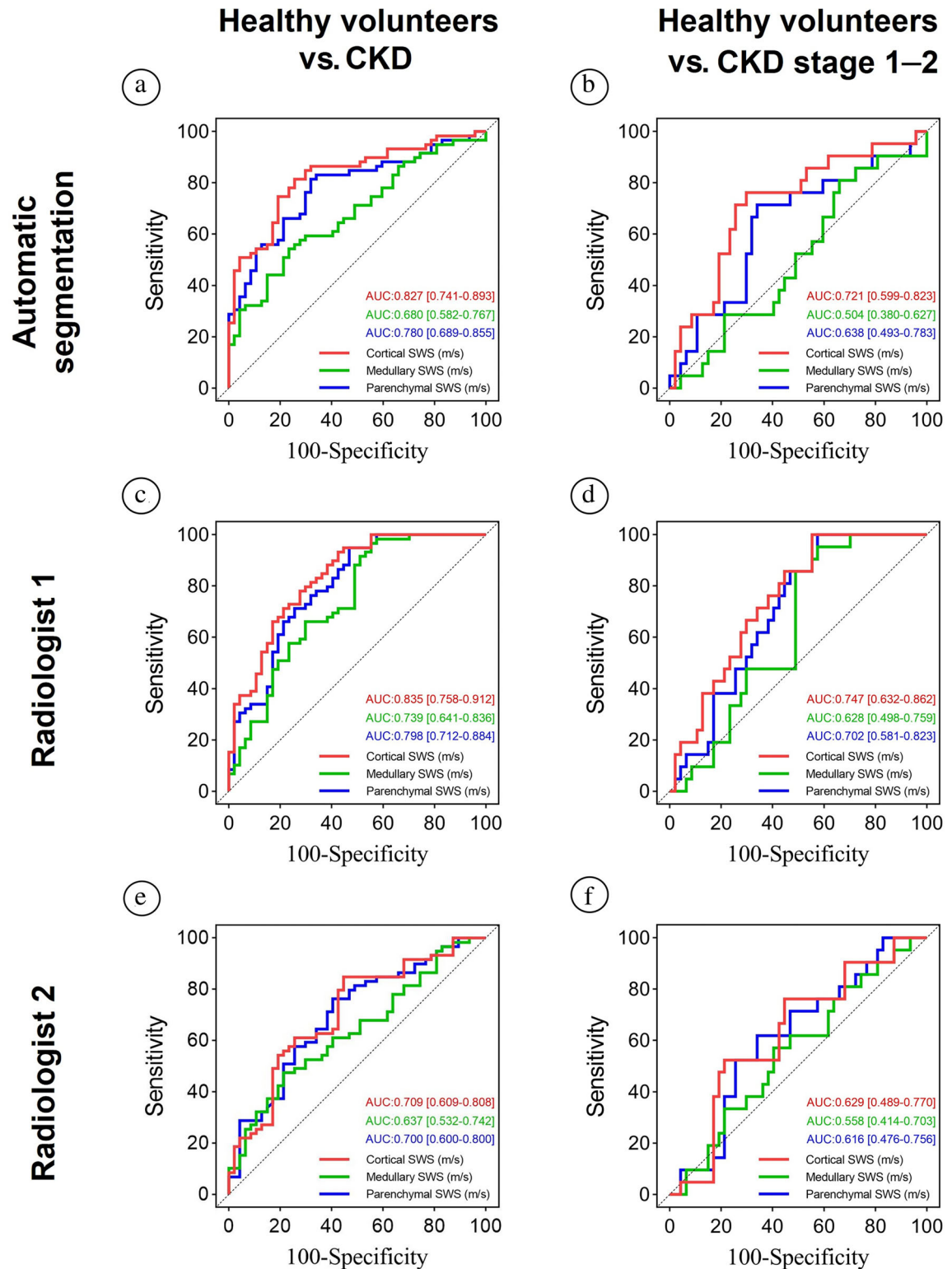


FIGURE 5: Diagnostic performance of the renal SWS values obtained via automatic quantification and via two radiologists using conventional manual quantification. Receiver operating characteristic curves for differentiating between healthy volunteers and participants with all CKD stages (a, c, e), and between healthy volunteers and participants with CKD stage 1–2 (b, d, f) are shown. SWS = shear wave speed; CKD = chronic kidney disease.

functions and is therefore more susceptible to pathological processes such as glomerulosclerosis and interstitial fibrosis in the CKD progression, which may lead to earlier changes in cortical stiffness.

### Limitations

First, no analysis was performed on CKD patients with different etiologies. Future in-depth analyses should be performed for patients with CKD with different etiologies to

**TABLE 5. Diagnostic Efficacy of Automatically Quantified Renal SWS Values in Identifying CKD Participants With Different Degrees of Impaired Renal Function**

	AUC	95% CI	Sensitivity (%)	Specificity (%)	Cutoff value (m/second)	<i>P</i>
Healthy volunteers ( <i>n</i> = 47) vs. CKD ( <i>n</i> = 59)						
Cortical SWS (m/second)	0.827	0.741–0.893	81.36	74.47	2.460	<0.001
Medullary SWS (m/second)	0.680	0.582–0.767	54.24	76.60	2.222	<0.001
Parenchymal SWS (m/second)	0.780	0.689–0.855	81.36	68.09	2.423	<0.001
Healthy volunteers ( <i>n</i> = 47) vs. CKD stage 1–2 ( <i>n</i> = 21)						
Cortical SWS (m/second)	0.721	0.599–0.823	76.19	70.21	2.484	0.001
Medullary SWS (m/second)	0.504	0.380–0.627	80.95	34.04	2.450	0.963
Parenchymal SWS (m/second)	0.638	0.493–0.783	71.43	65.96	2.433	0.070
CKD stage 1–2 ( <i>n</i> = 21) vs. CKD stage 3 ( <i>n</i> = 22)						
Cortical SWS (m/second)	0.669	0.509–0.805	72.73	66.67	2.392	0.048
Medullary SWS (m/second)	0.693	0.533–0.824	72.73	71.43	2.255	0.022
Parenchymal SWS (m/second)	0.701	0.543–0.831	77.27	66.67	2.340	0.015
CKD stage 3 ( <i>n</i> = 22) vs. CKD stage 4–5 ( <i>n</i> = 16)						
Cortical SWS (m/second)	0.835	0.679–0.935	87.50	81.82	2.238	<0.001
Medullary SWS (m/second)	0.767	0.602–0.888	75.00	86.36	2.095	0.002
Parenchymal SWS (m/second)	0.798	0.637–0.911	81.25	81.82	2.160	<0.001

For each pair of comparison, when the participant's renal SWS value is less than the cutoff value, CKD or a higher degree is diagnosed. SWS = shear wave speed; AUC = area under the curve; CI = confidence interval; *P* = significance level of comparison of AUC with that of random case (AUC = 0.500); CKD = chronic kidney disease.

explore the impact on renal stiffness. Second, renal puncture pathology results were lacking for the CKD patients. An increased sample size should also be performed to further improve the relevant histological validation. Third, our study recruited healthy volunteers based on previous health examinations and medical histories, which exhibit inadequate discipline and standardization. Laboratory data should be included in the future study. Fourth, there was an age mismatch between healthy volunteers and CKD groups in this study. To eliminate its potential impact on the results, age was used as a covariate in ANCOVA for intergroup comparisons. Future may align the ages of different populations to further improve the reliability of the conclusions. Fifth, although the segmentation performance in the CKD 4–5 group was relatively inferior compared to the other groups, but it remained adequate. Therefore, this did not affect the conclusion regarding abnormal renal stiffness in the CKD stage 4–5 group. In future studies, large models such as medical segment anything model trained on over one million medical images could be applied to improve performance.<sup>40</sup>

## Conclusion

mMRE combined with automatic segmentation may allow efficient assessment of renal function alterations in patients with CKD and has potential to diagnose early injury in CKD.

## Acknowledgments

This study has received funding from the Science and Technology Planning Project of Shenzhen Municipality, China (Award Number: JCYJ20230807094602006), Guangdong Medical Research Foundation, China (Award Number: A2024660), and the Shenzhen-Hong Kong Institute of Brain Science-Shenzhen Fundamental Research Institutions of China (Award Number 2024SHIBS0003).

## References

1. Sundström J, Bodegard J, Bollmann A, et al. Prevalence, outcomes, and cost of chronic kidney disease in a contemporary population of 2.4 million patients from 11 countries: The CaReMe CKD study. *Lancet Reg Health Eur* 2022;20:100438.



2. Wang L, Xu X, Zhang M, et al. Prevalence of chronic kidney disease in China: Results from the sixth China chronic disease and risk factor surveillance. *JAMA Intern Med* 2023;183(4):298-310.
3. Barrera-Chimal J, Lima-Posada I, Bakris GL, Jaisser F. Mineralocorticoid receptor antagonists in diabetic kidney disease—Mechanistic and therapeutic effects. *Nat Rev Nephrol* 2022;18(1):56-70.
4. Shlipak MG, Tummalaipalli SL, Boulware LE, et al. The case for early identification and intervention of chronic kidney disease: Conclusions from a Kidney Disease: Improving Global Outcomes (KDIGO) controversies conference. *Kidney Int* 2021;99(1):34-47.
5. Levey AS, Eckardt KU, Tsukamoto Y, et al. Definition and classification of chronic kidney disease: A position statement from Kidney Disease: Improving Global Outcomes (KDIGO). *Kidney Int* 2005;67(6):2089-2100.
6. Li DY, Yin WJ, Yi YH, et al. Development and validation of a more accurate estimating equation for glomerular filtration rate in a Chinese population. *Kidney Int* 2019;95(3):636-646.
7. Wang Y, Adingwupu OM, Shlipak MG, et al. Discordance between creatinine-based and cystatin C-based estimated GFR: Interpretation according to performance compared to measured GFR. *Kidney Med* 2023;5(10):1007-10.
8. Huang R, Fu P, Ma L. Kidney fibrosis: From mechanisms to therapeutic medicines. *Signal Transduct Target Ther* 2023;8(1):129.
9. Manduca A, Bayly PJ, Ehman RL, et al. MR elastography: Principles, guidelines, and terminology. *Magn Reson Med* 2021;85(5):2377-2390.
10. Selvaraj EA, Mózes FE, Jayaswal ANA, et al. Diagnostic accuracy of elastography and magnetic resonance imaging in patients with NAFLD: A systematic review and meta-analysis. *J Hepatol* 2021;75(4):770-785.
11. Zhang J, Yu Y, Liu X, et al. Evaluation of renal fibrosis by mapping histology and magnetic resonance imaging. *Kidney Dis* 2021;7(2):131-142.
12. Han JH, Ahn JH, Kim JS. Magnetic resonance elastography for evaluation of renal parenchyma in chronic kidney disease: A pilot study. *Radiol Med* 2020;125(12):1209-1215.
13. Güven AT, Idilman IS, Cebayilov C, et al. Evaluation of renal fibrosis in various causes of glomerulonephritis by MR elastography: A clinico-pathologic comparative analysis. *Abdom Radiol* 2022;47(1):288-296.
14. Brown RS, Sun MRM, Stillman IE, Russell TL, Rosas SE, Wei JL. The utility of magnetic resonance imaging for noninvasive evaluation of diabetic nephropathy. *Nephrol Dial Transplant* 2020;35(6):970-978.
15. Lang ST, Guo J, Bruns A, et al. Multiparametric quantitative MRI for the detection of IgA nephropathy using tomoelastography, DWI, and BOLD imaging. *Invest Radiol* 2019;54(10):669-674.
16. Marticorena Garcia SR, Grossmann M, Bruns A, et al. Tomoelastography paired with T2\* magnetic resonance imaging detects lupus nephritis with normal renal function. *Invest Radiol* 2019;54(2):89-97.
17. Streitberger KJ, Guo J, Tzschätzsch H, et al. High-resolution mechanical imaging of the kidney. *J Biomech* 2014;47(3):639-644.
18. Tzschätzsch H, Guo J, Dittmann F, et al. Tomoelastography by multi-frequency wave number recovery from time-harmonic propagating shear waves. *Med Image Anal* 2016;30:1-10.
19. Papazoglou S, Hirsch S, Braun J, Sack I. Multifrequency inversion in magnetic resonance elastography. *Phys Med Biol* 2012;57(8):2329-2346.
20. Dzyubak B, Venkatesh SK, Manduca A, Glaser KJ, Ehman RL. Automated liver elasticity calculation for MR elastography. *J Magn Reson Imaging* 2016;43(5):1055-1063.
21. Rezvani Habibabadi R, Khoshpouri P, Ghadimi M, et al. Comparison between ROI-based and volumetric measurements in quantifying heterogeneity of liver stiffness using MR elastography. *Eur Radiol* 2020;30(3):1609-1615.
22. Levey AS, Stevens LA, Schmid CH, et al. A new equation to estimate glomerular filtration rate. *Ann Intern Med* 2009;150(9):604-612.
23. Meyer T, Marticorena Garcia S, Tzschätzsch H, et al. Comparison of inversion methods in MR elastography: An open-access pipeline for processing multifrequency shear-wave data and demonstration in a phantom, human kidneys, and brain. *Magn Reson Med* 2022;88(4):1840-1850.
24. Marticorena Garcia SR, Grossmann M, Lang ST, et al. Tomoelastography of the native kidney: Regional variation and physiological effects on in vivo renal stiffness. *Magn Reson Med* 2018;79(4):2126-2134.
25. Dittmann F, Tzschätzsch H, Hirsch S, et al. Tomoelastography of the abdomen: Tissue mechanical properties of the liver, spleen, kidney, and pancreas from single MR elastography scans at different hydration states. *Magn Reson Med* 2017;78(3):976-983.
26. Isensee F, Jaeger PF, Kohl SAA, Petersen J, Maier-Hein KH. nnU-Net: A self-configuring method for deep learning-based biomedical image segmentation. *Nat Methods* 2021;18(2):203-211.
27. Taha AA, Hanbury A. An efficient algorithm for calculating the exact Hausdorff distance. *IEEE Trans Pattern Anal Mach Intell* 2015;37(11):2153-2163.
28. Dillman JR, Benoit SW, Gandhi DB, et al. Multiparametric quantitative renal MRI in children and young adults: Comparison between healthy individuals and patients with chronic kidney disease. *Abdom Radiol* 2022;47(5):1840-1852.
29. Rueden CT, Schindelin J, Hiner MC, et al. ImageJ2: ImageJ for the next generation of scientific image data. *BMC Bioinformatics* 2017;18(1):529.
30. Koo TK, Li MY. A guideline of selecting and reporting intraclass correlation coefficients for reliability research. *J Chiropr Med* 2016;15(2):155-163.
31. Bones IK, Bos C, Moonen C, Hendrikse J, van Stralen M. Workflow for automatic renal perfusion quantification using ASL-MRI and machine learning. *Magn Reson Med* 2022;87(2):800-809.
32. Xiao G, Zhu S, Xiao X, Yan L, Yang J, Wu G. Comparison of laboratory tests, ultrasound, or magnetic resonance elastography to detect fibrosis in patients with nonalcoholic fatty liver disease: A meta-analysis. *Hepatology* 2017;66(5):1486-1501.
33. Kim SW, Lee JM, Park S, et al. Diagnostic performance of spin-echo echo-planar imaging magnetic resonance elastography in 3T system for noninvasive assessment of hepatic fibrosis. *Korean J Radiol* 2022;23(2):180-188.
34. Liang Y, Li D. Magnetic resonance elastography in staging liver fibrosis in non-alcoholic fatty liver disease: A pooled analysis of the diagnostic accuracy. *BMC Gastroenterol* 2020;20(1):89.
35. Shatil AS, Kirpalani A, Younus E, Tyrrell PN, Krizova A, Yuen DA. Magnetic resonance elastography-derived stiffness predicts renal function loss and is associated with microvascular inflammation in kidney transplant recipients. *Transplant Direct* 2022;8(6):e1334.
36. Kirpalani A, Hashim E, Leung G, et al. Magnetic resonance elastography to assess fibrosis in kidney allografts. *Clin J Am Soc Nephrol* 2017;12(10):1671-1679.
37. Kriz W, Kaissling B. Structural organization of the mammalian kidney. In: Alpern RJ, Hebert SC, editors. *The Kidney: Physiology and pathophysiology*. 4th ed. Amsterdam: Academic Press; 2008. p 479-563.
38. Pi S, Li Y, Lin C, et al. Arterial spin labeling and diffusion-weighted MR imaging: Quantitative assessment of renal pathological injury in chronic kidney disease. *Abdom Radiol* 2023;48(3):999-1010.
39. Jiang K, Ferguson CM, Woollard JR, et al. Magnetization transfer imaging is unaffected by decreases in renal perfusion in swine. *Invest Radiol* 2019;54(11):681-688.
40. Ma J, He Y, Li F, Han L, You C, Wang B. Segment anything in medical images. *Nat Commun* 2024;15(1):654.